LA-UR -87-2653

CONF 8706192--1

Los Alamos National Lab. Pay operated by the University of California for the United States Department of Energy under contract W-7405-ENG-36

LA-UR--87-2553

DE87 014734

TITLE ANALYSIS OF UNDULATOR FIELD ERRORS FOR XUV FELS

AUTHOR(S) C. James Elliott
Brian D. McVey

SUBMITTED TO Physics Scripta
Proceedings of
Undulator Magnets for Synchrotron
Radiation and Free Electron Lasers
25-26 June, Trieste, Italy

Los Alamos National Laboratory
Los Alamos, New Mexico 87545

Analysis of Undulator Field Errors for XUV FELs *

C. James Elliott and Brian McVey
Los Alamos National Laboratory
Los Alamos, NM 87545, USA

Introduction

For a XUV FEL (extreme ultraviolet free electron laser), the magnetic field error analysis must specify how to keep the small signal gain to within $\sim 10^{-1}$ of the error free value. This contrasts with conventional undulator magnetic field error analysis that depends on qualatative criteria described by the STI group[1], or on properties of spontaneous emission studied by Kincaid[2]. The spontaneous emission is related to the gain of a FEL by Madey's theorem[3] when the gain is small, but it does not include a description of the requirements for radiating into the fundamental optical mode, nor does it apply to the large small-signal gain case.

In describing the field error requirements for a permenant magnet Halbach undulator[4] designed for operation at 12nm in the XUV, our starting point design has large small signal gain ≈ 5, significant energy spread $\approx 0.1\%$, moderate normalized emittance $\approx 2\pi$ mm-mrad, and a long undulator ≈ 12m. Our description also must include the 3-D wander of the electron beam in and out of the optical mode. Adequate modeling of all these effects is achieved by incorporation of a field error package into the FELEX code[5]

The differential equations used in FELEX have been averaged over an undulator wavelength, and this averaging removes steering errors from the equations. The steering errors give rise to an angular error $\Delta\theta_x$,

$$\Delta\theta_x = \frac{e}{mc\gamma}\int \delta B_y dz,$$

where δB_y is the magnetic field error along a length dz for a particle of charge e, mass m, and Lorentz factor γ. Taking δB_y to be sinusoidal and extending over the half period $(0, \lambda_w/2)$ gives rise to the Kincaid error model. For $k_w = 2\pi/\lambda_w$, it gives and angular error corresponding to the error field $\delta B_y = (mck_w\delta a_w/e)\sin(k_w z)$ of

$$\hat{\theta} = \Delta\theta_x = \frac{2\delta a_w}{\gamma} = \frac{2\hat{\epsilon} a_w}{\gamma},$$

where a_w is the scaled vector potential and $\hat{\epsilon}$ is the fractional error in the amplitude of a_w over the half period. This specific model of field errors does not include correlations of $\hat{\epsilon}$ from one half period to the next. For carefully engineered undulators, these correlations can be important and when taken into account can lead to an effective value of σ, the variance of $\hat{\epsilon}$, that is several times lower. This uncorrelated random error model, however,

* This work was supported by the Advanced Energy Projects Division, Office of Basic Energy Science, DOE

is the starting point for realistic field error analysis because of its simplicity and from the insights it brings.

In this work, the term *one plane focusing* is an idealization that refers to a plane parallel undulator with a magnetic field that depends only on axial location and horizontal position. The crucial motion of the electrons is in the vertical plane and is not subject to the focusing forces that affect the horizontal motion. Hence, the analysis of this plane includes no betatron forces. In contrast, the crucial electron motion in an undulator with two plane betatron focusing is subject to betatron forces. The study of field errors in non-perfect one plane focusing devices also includes errors that lead to motion in the vertical plane. Because this motion includes focusing forces, its analysis also falls under the category of betatron focusing. Furthermore, there is an additional difference in the phase equation between the canted pole approach[1] and the parabolic pole piece approach used in the FELEX calculations, even though both of these have two plane focusing.

The remainder of this paper is divided into three sections: no betatron focusing, betatron focusing, and conclusions. The no betatron focusing results study spontaneous emission from the sum-of-phasor representation and shows how the amplitude of spontaneous emission for a cold resonant beam depends on the single parameter called the longitudinal coherence phase, Φ_l. Based upon these results, a scaling diagram is constructed showing where wander and longitudinal coherence are important. The betatron focusing results have three subsections. The first deals with the random walk problem including betatron focusing. The second addresses the benefit that can accrue from use of a solenoidal guide field. The last subsection gives the results of numerical simulations. These numerical results: contain examples of wander in phase space, give the gain for random undulators, show the improvement for a solenoidal field, show the advantage derivable from adding steering corrector segments, and give the variation of gain with Φ_l and number of correcting elements for the 12mm XUV FEL design.

No Betatron Focusing

First we present a simplified approach to calculation of the degradation of spontaneous emission in a wiggler without betatron focusing. This method breaks the continuous integral over the wiggler in a sum over half periods. We add up the phasors directly rather than rely on the Rice-Mandel[2] approximation. This work shows that a single parameter, the longitudinal coherence phase that we designate by Φ_l, describes the degradation of intensity as averaged over single particle realizations of the trajectories.

We start with an expression for the optical field at frequency ω_s radiated by a single particle

$$E \propto \int_0^T \hat{n} \times (\hat{n} \times \hat{\beta}) \exp\left[i\omega_s \left(t - \hat{n} \cdot \vec{r}(t)/c \right) \right] dt.$$

We take $\hat{n}$ in the x direction and examine E_z,

$$E_z \propto \int_0^T dt \beta_z \exp\left[i\omega_s \left(t - z(t)/c \right) \right],$$

and we approximate β_z by the resonant term

$$\beta_z \approx \frac{a_w}{\gamma} \sin k_w z \approx \frac{a_w}{2i\gamma} \exp\left[ik_w z(t) \right].$$

At large γ the transit time over half a period is uniform; furthermore, the variation of the combined phase terms is small over half a period and to good approximation we have the sum-of-phasor representation

$$I \propto \sum_{n=1}^{2N_u} \exp(i\phi_n),$$

where

$$\phi_n = \int_{z_{n-1/2}}^{z_{n+1/2}} dz\,(\omega/\beta_z - k_u - k_r),$$

and where the field errors cause random variations in β_z. Here $z_{n\pm1/2}$ is the centered axial location of the nth half period cell, and k_r is the wavenumber corresponding to ω_r, $k_r = \omega_r/c$. Writing

$$\frac{1}{\beta_z} = \frac{1}{\beta_{z0}} + \delta\left(\frac{1}{\beta_z}\right),$$

and choosing the resonant condition

$$\frac{\omega}{\beta_{z0}} = (k_u + k_r)c,$$

or the more familiar form

$$\lambda_r = \frac{\lambda_u}{2\gamma^2}(1 + a_u^2/2),$$

we conclude

$$\phi_n = \int_{z_{n-1/2}}^{z_{n+1/2}} dz\,k_r\delta\left(\frac{1}{\beta_z}\right),$$

where we have taken $\beta_{z0} \approx 1$. With no field errors, $\phi_n = 0$, and all the $2N_u$ phasors add coherently.

To evaluate the effect of field errors, we examine the axial velocity that has been averaged over a half period,

$$\beta_z = 1 - \frac{1}{2\gamma^2}\left(1 + \frac{a_u^2}{2}\right) - \frac{1}{2}\beta_{x,\mathrm{rms}}^2 - \cdots$$

$$\beta_z = \frac{1}{2\gamma^2}a_u^2\left(\frac{\delta a_u}{a_u}\right) - \frac{1}{2}\beta_{x,\mathrm{rms}}^2$$

The $\delta a_u / a_u$ term is the amplitude phase term that is small for operation on the fundamental. Later we will justify this approximation. That leaves

$$\delta\beta_z \approx -\frac{1}{2}\beta_{x,\mathrm{rms}}^2$$

where if we split the undulator up into $2N_u$ segments and denote $\beta_{z,n}$ as the value on the nth segment, we have

$$\beta_{z,n} = \beta_{z,n-1} - \frac{2a_u}{\gamma^2}\left(\frac{\delta a_u}{a_u}\right)_{n-1}$$

Combining the above and $\langle \xi_n \ldots a_n \rangle \ldots \xi_n$ gives us

$$\phi_n = \frac{N_u k}{2} a_u^2 \sigma^2 \left[\frac{1}{2}\xi_n + \sum_{m=1}^{n-1} \xi_m \right].$$

where

$$\xi_n = \left[\sum_{m=1}^{n} u_m \right]^2$$

Here u_m has zero mean and a variance of unity, and that implies that $\langle \xi_n \rangle = n - 1$. Defining ϕ_{2N_u} as Φ_l, the longitudinal coherence phase, we have

$$\Phi_l = \frac{N_u k\, a_u^2 \sigma^2}{2} 2N_u .$$

This expression can also be written in the more general form that applies even in the presence of a solenoidal focusing field, as we indicate later

$$\Phi_l = \frac{k}{2} \theta^2 \int_0^{L_u} \frac{z}{\Delta z} dz.$$

Upon using the resonance condition for the n_h harmonic, we have

$$\Phi_l = \frac{\pi a_u^2}{1 + a_u^2 / 2} \sigma^2 N_u^2 n_h .$$

The higher harmonics that occur in spontaneous emission accrue from the periodic variation in β_z and the anti-resonant term we dropped, but the over all form for them is the same as the fundamental ($n_h = 1$), except for the factor[2] of n_h. We can now write the expression for the n'th phase in terms of the longitudinal coherence phase and the number of wiggler periods as

$$\phi_n = \frac{\Phi_l}{2N_u^2} \left[\frac{1}{2}\xi_n + \sum_{m=1}^{n-1} \xi_m \right].$$

We can go back and estimate the contribution to ϕ_n of the amplitude term we dropped earlier. The dropped term taken by itself would have produced a value of ϕ_{2N_u} we call ϕ_A.

$$\phi_A = \frac{1}{2\gamma^2} a_u^2 \frac{k \lambda_u}{2} \sigma \sum_{m=1}^{2N_u} u_m .$$

$$= \pi \frac{a_u^2}{1 + a_u^2 / 2} \sigma \sum_{m=1}^{2N_u} u_m$$

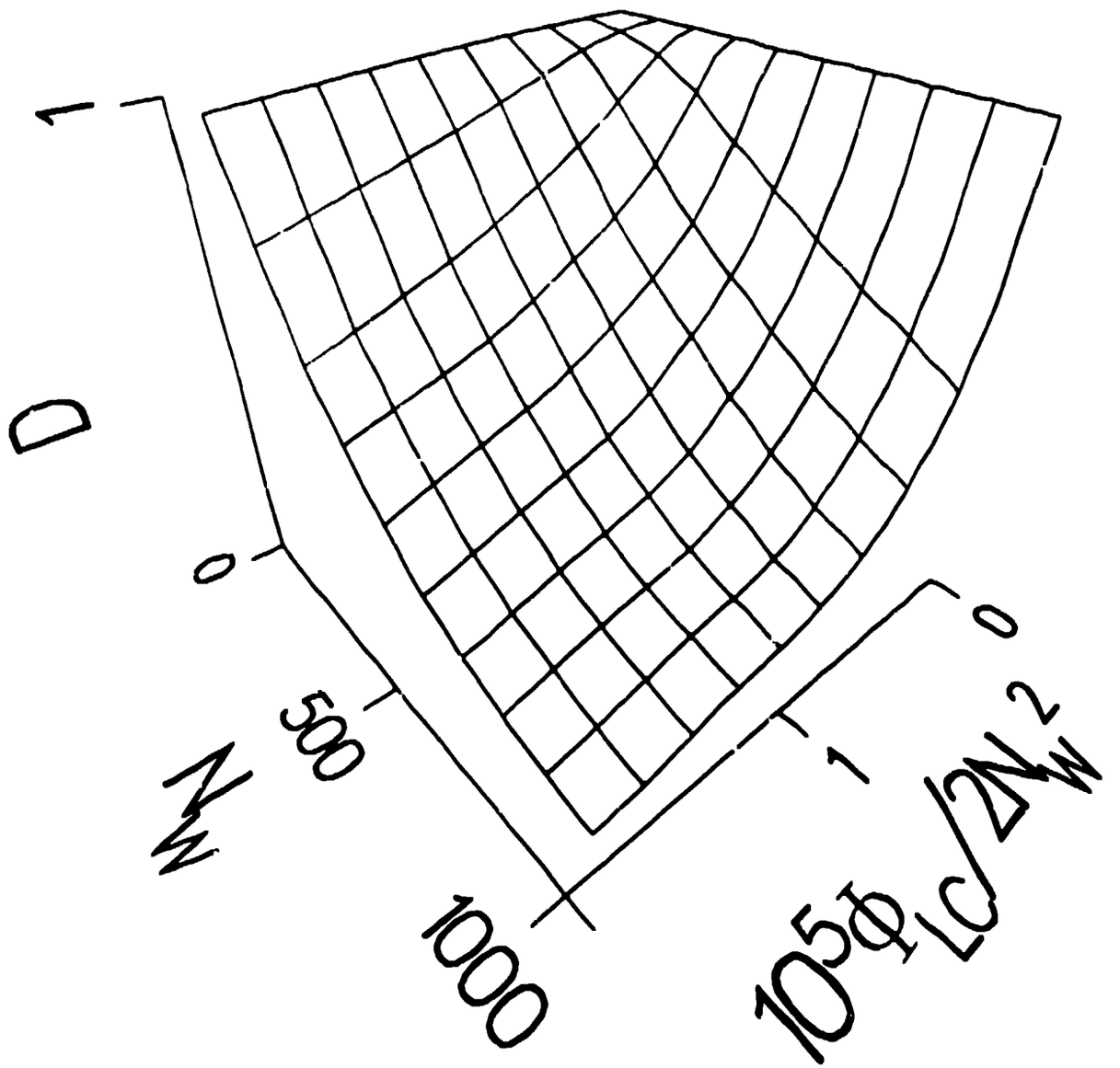

Fig. 1. The degradation of spontaneous emission at the no error resonant condition plotted as a function of the number of undulator periods and a scaled longitudinal phase

This quantity has zero mean and a variance

$$\sigma_a^2 \quad \left(\frac{n_b \pi a_u^2 \sigma}{1 + a_u^2/2} \right)^2 2N_w .$$

Because $n_b \sigma^2 N_w^2 = 1$ arises from the requirement that $\Phi_L = 1$, it follows that $\langle \sigma_a^2 \rangle = n_b N_w$, and this amplitude phase is unimportant for many period undulators or low harmonics.

We now plot the degradation, D, of the intensity as a function of N_w and $\Phi_L 2N_w^2$. This is shown in Fig. 1. Here, we have taken n_{w_j} to be a gaussian random variable of

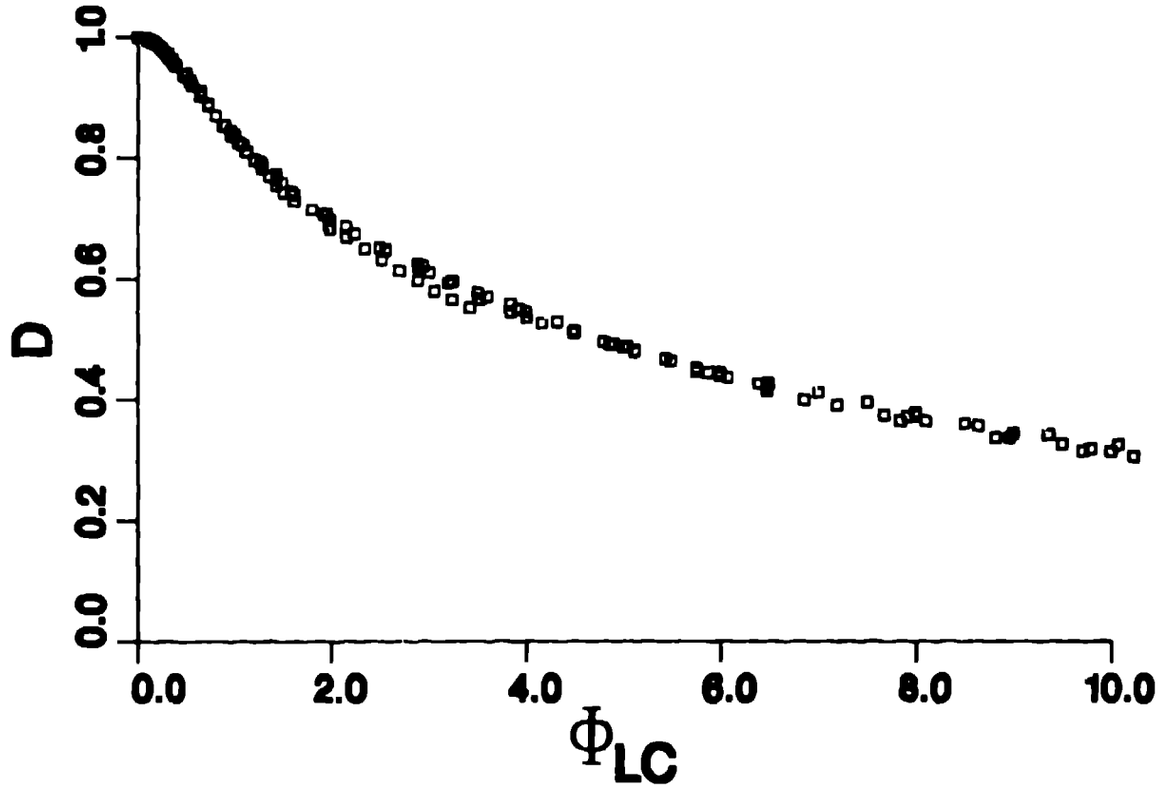

Fig. 2. A plot of the information in Fig. 1 in terms of the single parameter Φ_{LC}.

zero mean and unity variance. We have averaged over 100 different random undulators to approximate the definition of D

$$D \quad \left\langle \sum_{n=1}^{2N_u} \exp\left(i\phi_n\right)^2 \right\rangle / 4N_u^2 .$$

Here we have taken $N_u = 100, 200, \ldots 1000$.

Now, we expect D to be a function of Φ_{LC} only, as $N_u \to \infty$. We have replotted the same data from Fig. 1 in Fig. 2 as a function of Φ_{LC}, making no distinction between the different values of N_u. The variation we see in Fig. 2 is attributed to imperfect statistics and finite N_u.

The major conclusion we reach within this model is that the degradation D is, to good approximation, a function of Φ_{LC} only. The measure of the longitudinal coherence degradation is thus Φ_{LC}, and it is this same quantity that measures the mean angle of the $2N_u$ phasors that we add up to produce the spontaneous emission.

This model has, of course, a number of weaknesses in considering the coherence requirements for a FEL. First, the method treats a mono energetic electron beam. Second, for it to be relevant to the gain by Madey's theorem, the gain must be small, and this is not the case for the XUV. Third, the emittance of the electron beam may be important.

Fourth, the light must be emitted into the FEL mode, and this effect is not addressed. Fifth, the focusing forces, on the trajectories subject to them, need to be considered. Sixth, the effect of correction elements has not been evaluated. Seventh, the variation with respect to frequency of the spontaneous emission has not been considered. All of these requirements lead to the need for a comprehensive treatment using a computer code such as FELEX.

Before going on to FELEX, we can make an important general observation. In the coherent case, the two major considerations of getting a FEL to operate can be expressed in terms of some criterion for Φ_{lc} and another criterion for beam wander. This latter condition insures the electrons do not leave the optical mode. In the no betatron focusing case, a special case of the betatron focusing results presented later, the mean displacement of an electron from the axis is zero, and its standard deviation is

$$\langle x^2 \rangle^{1/2} = \langle \theta^2 \rangle^{1/2} \left(\frac{z}{\lambda_w/2} \right)^{1/2} \frac{z}{\sqrt{3}},$$

where

$$\langle \theta^2 \rangle^{1/2} = \frac{2a_w \sigma}{\gamma},$$

is the standard deviation of the angular kick per half wavelength of the undulator. This result is in agreement with Ref. 2. Thus, we require

$$\langle x^2 \rangle^{1/2} \leq w_0,$$

where w_0 is the optical beam waist parameter, and

$$\Phi_{lc} \leq \Phi_{max}.$$

Here Φ_{max} depends on all the physics associated with the actual FEL, and may be different from that determined by the simple model given above.

One important feature of the no betatron results emerges from the scaling of these two requirements with respect to error levels and the number of periods (or length) of an undulator. For the longitudinal coherence, the expression for Φ_{lc} indicates the scaling goes as

$$\sigma \propto N_w^{-1},$$

and for the beam wander the $\langle x^2 \rangle$ expression gives

$$\sigma \propto N_w^{-1.5}.$$

These scalings are shown in Fig. 3 where we see that for a large number of periods in the undulator, beam wander dominates in determining the errors and for a small number of periods, longitudinal coherence dominates. The errors increase in going to the right on the abscissa until a given point encounters either of the two curves. Thus, the region between the origin and the two curves plotted is the safe region, and beyond either of the two curves is the danger region. If the number of periods in the undulator is too great, segmentation

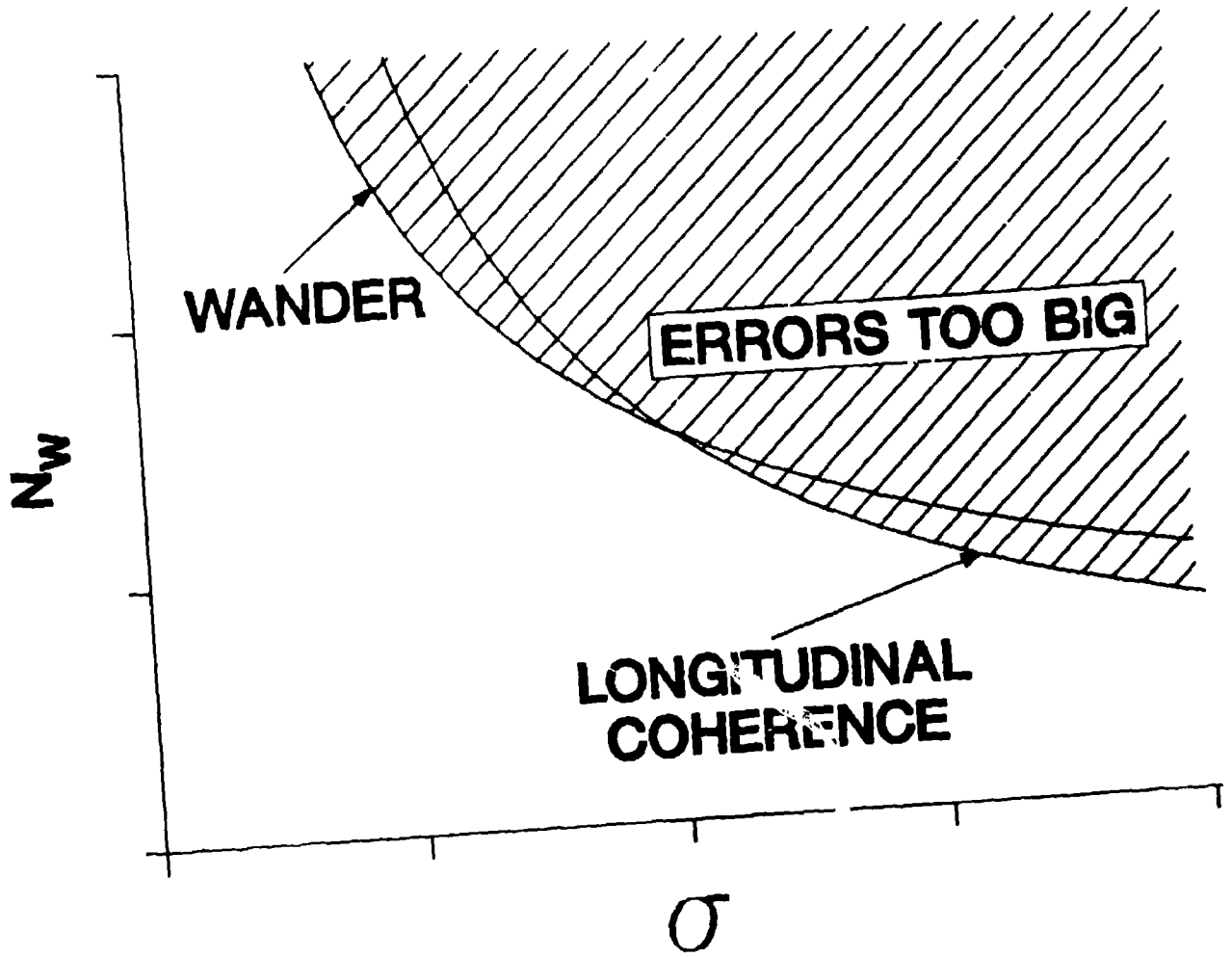

Fig. 3. The scaling of undulator periods versus magnetic field error level. The shaded region is where errors reduce the gain excessively. For many period undulators, electron beam wander is the constraint that is most critical, but for few period undulators, longitudinal coherence is the most critical constraint.

of the undulator can be considered, where steering corrections are applied to each segment. Then the number of periods in each segment is the relevant parameter, and we move toward the region where the longitudinal coherence is the more important quantity. These general features will also be seen by example to apply to two plane focusing.

Betatron Focusing

Here we examine two analytical cases and report on a number of numerical simulations. The first analytical case is the random walk in the presence of betatron focusing. Next we analyze the addition of a solenoidal magnetic field. Finally we examine simulations of a number of cases all of which address the Los Alamos 12m 120nm XUV design[7]. The first case we examine is without steering error corrections, and we show a case where addition of a solenoidal field helps to a point of reduced beam wander. Finally we show the effect

of adding steering corrector segments.

Random walk with betatron focusing

The random walk problem in x, x' space with focusing can be cast as follows

$$\begin{pmatrix} x \\ x' \end{pmatrix}_{n+1} = \begin{pmatrix} 0 \\ \hat{\theta}_n \end{pmatrix} + \begin{pmatrix} \cos\theta & \sin\theta / k_{\beta x} \\ k_{\beta x} \sin\theta & \cos\theta \end{pmatrix} \begin{pmatrix} x \\ x' \end{pmatrix}_n .$$

Here $\Delta z = \lambda_w / 2 = \sin\theta / k_{\beta x}$ determines the betatron angle, θ, traversed in a half period. The random angular kick $\hat{\theta}_n$ is introduced on the n'th step. With $\hat{\theta}_n = 0$, the pure betatron motion is recovered. The betatron wavenumber $k_{\beta x}$ depends on the details of the magnetic field[5]. For this work, we assume the magnetic field has the transverse dependence

$$B_y \propto b_0 \left(1 - \frac{k_x^2 x^2}{2} - \frac{k_y^2 y^2}{2} \right) + \mathcal{O}(x^3, y^3),$$

and a sinusoidal longitudinal dependence. Then

$$k_{\beta x} = (\beta_x)_{rms} k_x ,$$

$$k_{\beta y} = (\beta_x)_{rms} k_y ,$$

where

$$(\beta_x)_{rms} = \frac{a_w}{\sqrt{2}\gamma} .$$

Starting with

$$\begin{pmatrix} x \\ x' \end{pmatrix}_0 = \begin{pmatrix} 0 \\ 0 \end{pmatrix},$$

the solution of the difference equation is

$$\begin{pmatrix} x \\ x' \end{pmatrix}_n = \sum_{j=0}^{n-1} \begin{pmatrix} k_{\beta x}^{-1} \sin j\theta \\ \cos j\theta \end{pmatrix} \hat{\theta}_{n-1-j} .$$

Using $\langle \hat{\theta}_n^2 \rangle = \langle \hat{\theta}^2 \rangle$, we can form the variance

$$\left\langle \begin{pmatrix} x^2 \\ x'^2 \end{pmatrix}_n \right\rangle = \langle \hat{\theta}^2 \rangle \sum_{j=0}^{n-1} \begin{pmatrix} k_{\beta x}^{-2} \sin^2 j\theta \\ \cos^2 j\theta \end{pmatrix} .$$

which we approximate as an integral

$$\left\langle \begin{pmatrix} x^2 \\ x'^2 \end{pmatrix}_n \right\rangle = \langle \hat{\theta}^2 \rangle \int_0^{k_{\beta x} z} \begin{pmatrix} k_{\beta x}^{-2} \sin^2 \Phi \\ \cos^2 \Phi \end{pmatrix} \frac{d\Phi}{k_{\beta x} \Delta z} .$$

Thus, upon integration, we conclude

$$\begin{pmatrix} x^{2}{}^{1}{}^{2} \\ x'^{2}{}^{1}{}^{2} \end{pmatrix} \quad \frac{1}{\sqrt{2}}\,\theta^{2}{}^{1}{}^{2}\left(\frac{z}{\Delta z}\right)^{1}{}^{2}\begin{pmatrix} k_{\beta x}^{-1}(1 \quad \sin 2\Phi/2\Phi)^{1}{}^{2} \\ (1 \quad \sin 2\Phi/2\Phi)^{1}{}^{2} \end{pmatrix},$$

where $\Phi \quad k_{\beta x} z$.

In the limit that $\Phi \to 0$, the betatron forces do not have time to act and it is

$$\begin{pmatrix} x^{2}{}^{1}{}^{2} \\ x'^{2}{}^{1}{}^{2} \end{pmatrix} \quad \frac{1}{\sqrt{2}}\,\theta^{2}{}^{1}{}^{2}\left(\frac{z}{\Delta z}\right)^{1}{}^{2}\begin{pmatrix} 2z/\sqrt{6} \\ \sqrt{2} \end{pmatrix},$$

the same as the result without betatron focusing that we quoted from previously. Note the qualatative difference with the $\Phi \to \infty$ case where

$$\begin{pmatrix} x^{2}{}^{1}{}^{2} \\ x'^{2}{}^{1}{}^{2} \end{pmatrix} \quad \frac{1}{\sqrt{2}}\,\theta^{2}{}^{1}{}^{2}\left(\frac{z}{\Delta z}\right)^{1}{}^{2}\begin{pmatrix} k_{\beta x}^{-1} \\ 1 \end{pmatrix}.$$

In the latter case, both $x^{2}{}^{1}{}^{2}$ and $x'^{2}{}^{1}{}^{2}$ vary as $z^{1}{}^{2}$ and $x^{2}{}^{1}{}^{2} \quad k_{\beta x}^{-1} x'^{2}{}^{1}{}^{2}$. Also in this case we see that the angular efficiency is $1/\sqrt{2}$ compared to the no-betatron focusing case. The displacement variance is just the lever arm $k_{\beta x}^{-1}$ times the angular variance. In the $\Phi \to 0$ case, the lever arm is $z/\sqrt{3}$ instead of $k_{\beta x}^{-1}$ in the $\Phi \to \infty$ case. The net result of a long undulator with betatron focusing is to decrease the angular variance by a factor of $1/\sqrt{2}$ and the replace the lever arm $z/\sqrt{3}$ by $k_{\beta x}^{-1}$.

We can interpret the $\Phi \to \infty$ result in a phase space plot shown in Fig. 4. Suppose we introduce an angular error $\delta x'$ in phase space at point P, moving the point to P'. Without any more errors the point P' would continue to rotate around the phase space circle at constant radius. When it rotates 90° to point P'', we see that the error no longer is manifest as an angular error, but rather, is equivalent to a displacement error. This effect accounts for the diminished angular variance. Also, the lever arm of $k_{\beta x}^{-1}$, appears in this example because $\delta x(P'') \quad \delta x'(P') \cdot k_{\beta x}$. On average, for many transits around the circle, the square of the displacement is related to the square of the angular change by the square of the lever arm.

Solenoid with balanced betatron focusing

The transverse equations of motion in the presence of an axial magnetic field B_z and cyclotron frequency $\Omega \quad eB_z/mc$, are given by the differential equations

$$x'' \quad k_{\beta x}^{2} x + (\Omega/c) y',$$

$$y'' \quad k_{\beta y}^{2} y \quad (\Omega/c) x'.$$

These equations have a constant of motion

$$\omega \quad k_{\beta x}^{2} x^{2} + k_{\beta y}^{2} y^{2} + x'^{2} + y'^{2},$$

whose derivative is zero. That is, the addition of the solenoidal field preserves the constancy of the longitudinal derivative of the phase of a single particle and does not cause it to jitter

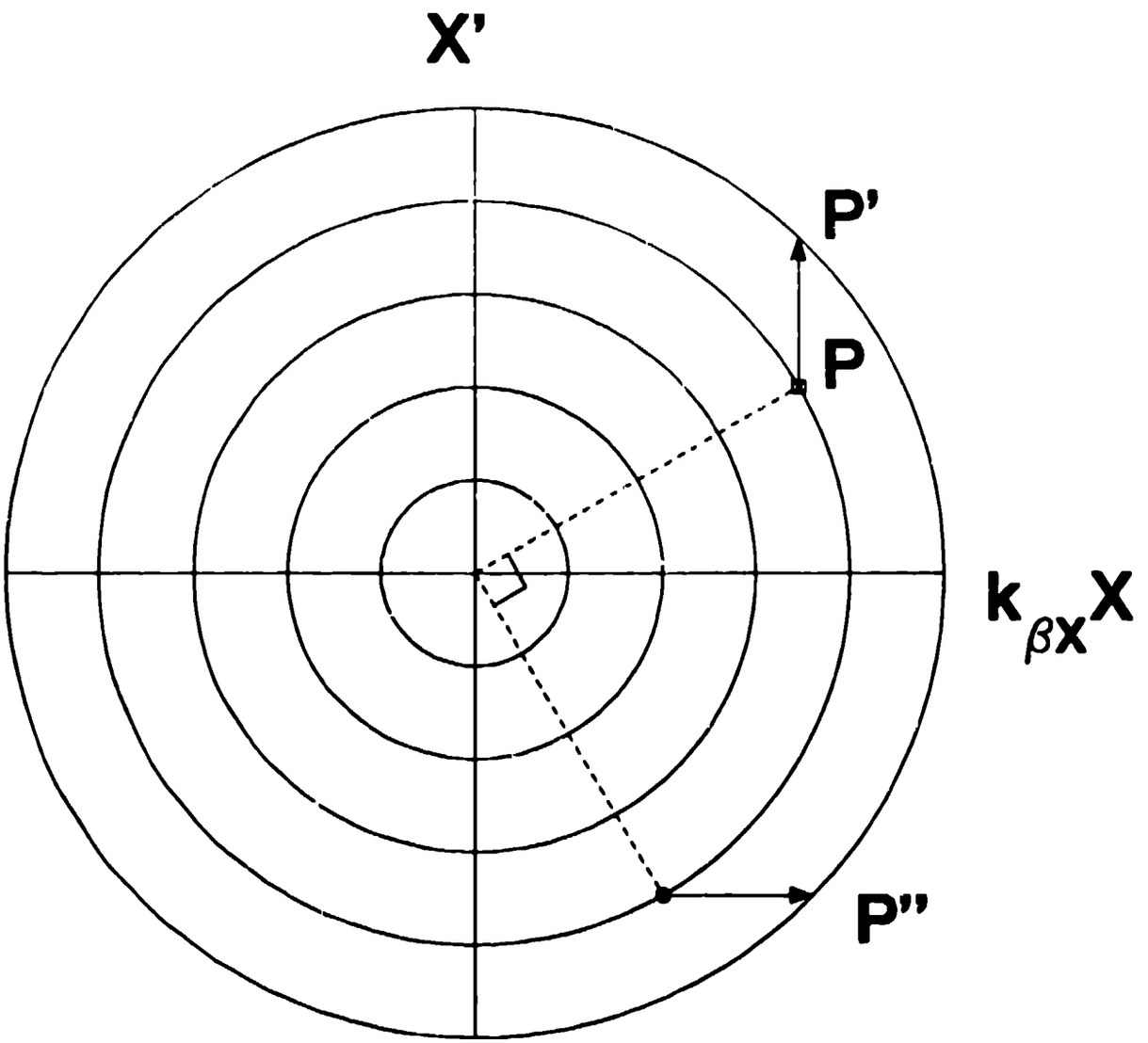

Fig. 4 The error PP' gets rotated by 90° and changes from an angular error to the equivalent of a displacement error.

back and forth in phase space. Thus, the attractive property of betatron focusing in two planes pointed out by Scharlemann[8] extends to the case where a solenoidal field has been added to the undulator.

Because of the focusing properties of the solenoid, we are interested in examining what happens to random error propagation. This we can do very simply when balanced betatron focusing occurs with $k_{\beta x}$ $k_{\beta y}$ k_β. Then the equations of motion can be rewritten as

$$u'' \quad k_\beta^2 u \quad i\Omega u' \quad c,$$

where

$$u \quad x \cdot iy.$$

Writing $u(0) \quad u$ and $u'(0) \quad u'_{\cdot}$, the general solution is

$$u \qquad \frac{(i\alpha \quad u_{\cdot} \quad u')\exp i\alpha_{\cdot} z \; + \; (i\alpha_{\cdot} u \qquad u')\exp i\alpha \quad z}{i(\alpha_{\cdot} \quad \alpha \quad)} ,$$

where

$$\alpha_{\cdot} \qquad \frac{\Omega_{\cdot} c \qquad \setminus (\Omega_{\cdot} c \cdot \quad 4 \cdot z}{2} .$$

The general solution can be written

$$\begin{pmatrix} u \\ u' \end{pmatrix} \quad M \begin{pmatrix} u \\ u'_{\cdot} \end{pmatrix} .$$

$$M \quad \begin{pmatrix} M_{11} & M_{12} \\ M_{21} & M_{22} \end{pmatrix} .$$

$$M_{11} \quad (\alpha_{\cdot} \exp i\alpha \quad z \quad \alpha \quad \exp i\alpha_{\cdot} z)\,'(\alpha_{\cdot} \quad \alpha \quad),$$

$$M_{12} \quad (\exp i\alpha_{\cdot} z \quad \exp i\alpha \quad z)\,'i(\alpha_{\cdot} \quad \alpha \quad),$$

$$M_{21} \quad i\alpha_{\cdot} \alpha \; (\exp i\alpha \quad z \quad \exp i\alpha_{\cdot} z)\,'(\alpha_{\cdot} \quad \alpha \quad),$$

$$M_{22} \quad (\alpha_{\cdot} \exp i\alpha_{\cdot} z \quad \alpha \quad \exp i\alpha \quad z)\,'(\alpha_{\cdot} \quad \alpha \quad).$$

Note that

$$M \quad \exp \quad i\Omega z \quad c,$$

and the transitive property holds

$$M(z_1)M(z_2) \quad M(z_1 \cdot z_2).$$

Following the previous development for random walk with betatron focusing we have

$$\begin{pmatrix} u \\ u' \end{pmatrix}_{n} \quad \sum_{j \quad 0}^{n \quad 1} M(j\Delta z) \begin{pmatrix} 0 \\ \hat{\theta}_n \quad 1 \quad j \end{pmatrix} .$$

Now u has real part x and imaginary part y, and M has real part M_r and imaginary part M_i. This translates the above equation into

$$\begin{pmatrix} x \\ x' \end{pmatrix}_{n} \quad \sum_{j \quad 0}^{n \quad 1} M_r(j\Delta z) \begin{pmatrix} 0 \\ \hat{\theta}_n \quad 1 \quad j \end{pmatrix} .$$

and

$$\begin{pmatrix} x^2 \\ x'^2 \end{pmatrix} = \frac{\hat{\theta}^2}{\Delta z} \int_{0}^{z} dz \begin{pmatrix} M_{r12}^2(z) \\ M_{r22}^2(z) \end{pmatrix} .$$

Similarily,

$$\begin{pmatrix} x^2 & y^2 \\ x'^2 & y'^2 \end{pmatrix} \approx \frac{\hat{\theta}^2}{\Delta z} \int_0^z dz \begin{pmatrix} M_{12}^{\ 2}(z) \\ M_{22}^{\ 2}(z) \end{pmatrix}.$$

Furthermore,

$$k_\beta^2 M_{12}^{\ 2} \quad M_{22}^{\ 2} \quad 1,$$

so that

$$\Phi_x \quad \Phi_y \quad \frac{\hat{\theta}^2}{\Delta z} z.$$

A simple interpretation of this result shows that it holds even without balanced betatron focusing. The quantity σ_x remains constant until it is altered by a field error. When the uncorrelated field error occurs, $x' \to x' + \hat{\theta}_n$ and $\Delta x'^2 \to \hat{\theta}^2$ on each step. The number of such steps is just $z/\Delta z$, giving the above result. Because the longitudinal coherence phase, Φ_{lc}, is just $k_z/2$ times the z integral of Φ_x, this result implies that it makes no difference what the solenoidal field level is; the expected longitudinal coherence is the same.

We are also interested in how the variances of the angular and displacement errors are distributed. Evaluating the integral shows

$$\langle x^2 + y^2 \rangle \quad \frac{\langle \hat{\theta}^2 \rangle}{\Delta z} \frac{2}{(\alpha_+ - \alpha_-)^2} \left[z - \frac{\sin(\alpha_+ - \alpha_-)z}{\alpha_+ - \alpha_-} \right],$$

and for large z,

$$\langle x^2 + y^2 \rangle \sim \langle \hat{\theta}^2 \rangle \frac{z}{\Delta z} \frac{2}{4k_\beta^2 + (\Omega/c)^2}.$$

Here we see that the variance of the radius decreases as the solenoidal field increases. But because of the constancy of Φ_x, we have

$$\langle x'^2 + y'^2 \rangle \sim \langle \hat{\theta}^2 \rangle \frac{z}{\Delta z} \frac{2k_\beta^2 + (\Omega/c)^2}{4k_\beta^2 + (\Omega/c)^2}.$$

We see that although $\langle x^2 + y^2 \rangle$ decreases with Ω, $\langle x'^2 + y'^2 \rangle$ increases by a factor of two as Ω increases from 0 to ∞, keeping Φ_x independent of Ω.

If control of beam wander is a problem, a solenoidal field can correct the situation without adversely affecting longitudinal coherence. Later we show a particle simulation that gives an example of this situation.

FELEX calculations

The equations of motion used in FELEX have been described elsewhere[5], and we augment these through two methods. The FELEX equations are obtained by averaging the equations of motion of the particle over the magnetic field wavelength. The field errors are of two types: (1) those adiabatic errors that appear in these averaged equations which vary slowly over a period and (2) those diabatic terms that do not appear in the averaged equations and require new terms.

The diabatic term is modeled[2] as we described in the introduction. This model assumes an error exists in the scaled vector potential of the form

$$\delta a_u = \delta\left(\frac{eB_u}{k_u mc}\right) = a_u \epsilon(z)\cos k_u z,$$

where $\epsilon(z)$ has a constant value ϵ_i for

$$(2n-1)(\pi/2) < k_u z < (2n+1)\pi/2,$$

whose mean is zero and variance is σ. This is a series of half period errors, each of which results in an angular deflection or steering of

$$\delta\theta = \frac{2\epsilon_i a_u}{\gamma},$$

and a negligable displacement. This angular deflection is added to the existing equation in FELEX for the angular evolution

$$\frac{d\gamma\beta_x}{dct} = \left(\frac{d\gamma\beta_x}{dct}\right)_0 + \frac{4a_w}{\lambda_w}\epsilon_i\sqrt{\lambda_w/2\Delta z},$$

where $\Delta z = c\Delta t$ is a variable integration step. Here

$$\epsilon_i = \sigma(1-2\hat{r})\sqrt{3},$$

where $\hat{r}$ is a random number distributed uniformly between 0 and 1 that gives ϵ_i a zero mean and a variance of σ. The change $2a_w\epsilon_i$ accrues to $\gamma\theta_x$ over the distance $\lambda_w/2$, where we take $\Delta z = \lambda_w/2$. The last term $\sqrt{\lambda_w/2\Delta z}$ extends the algorithm to arbitrary step size, keeping the standard deviation of β_x an invariant function of ct.

In constrast to the diabatic steering error term, the adiabatic term describes the phase errors. These are separately modeled without adding additional terms to the magnetic field but by specifying a magnetic field $B_y(z)$ where the z dependence describes the errors in the field. At 0.7% random errors in $B_y(z)$ with $\Delta z = \lambda_w/2$, less than 1% change occurred to the gain. Therefore, these errors were judged to be inconsequential. We reached a similar conclusion in our no betatron focusing analysis that showed $\langle\phi_n^2\rangle$ is small. Hence forth, we consider only the diabatic steering error terms.

Specific calculations for the Los Alamos 12m 120mm free-electron laser design[7] were made using FELEX. The input parameters are shown in Table I.

Table I

e-beam:	current	I	150A
	Lorentz factor	γ	1046
	energy spread	$\Delta E/E$	0.1%
	normalized emittance	$\gamma\epsilon'_x = \gamma\epsilon'_y$	247mm-mrad
undulator:	magnetic field	B	0.75T
	length	L_u	12m
	wavelength	λ_u	1.6cm
	focusing	balanced	
	field error	σ	0.1%,0.7%
optical:	wavelength	λ_s	12mm
	input power	P_{in}	90W
	Rayleigh range	z_r	3m

The random field error level, σ, is initially taken to be the advanced state-of-the art value of 0.1%, but when steering correction segments are considered for an ensemble of undulators, calculations are done for easily obtainable[1,2,9] values of 0.7%. Random undulators are generated using different random number seeds. The x, x' and y, y' emittance values ϵ'_x and ϵ'_y are the areas in phase space that include 86% of the particles, and the energy spread $\Delta E/E$ is the full width between the e^{-1} points of a gaussian distribution that includes 84% of the beam.

In Figs. 5 and 6 we show the accrued displacement and angular error of the e-beam for one random choice of field errors with $\sigma = 0.1\%$. In Fig. 5 the width of the beam is plotted versus the axial location within the undulator. The dashed lines are $\langle y \rangle \pm \sqrt{\langle 2y^2 \rangle}$, where the average is over the particles. These lines show that the y-motion is unaltered by the field errors considered. The measure, $\sqrt{\langle 2y^2 \rangle}$, gives the $1/e$ width initially when the e-beam is gaussian. Likewise, the solid lines are $\langle x \rangle \pm \sqrt{\langle 2x^2 \rangle}$. Because the equations of motion have been averaged over an undulator period, the rapid sinusoidal variation does not appear. The angular variables β_x and β_y are averaged over the particles to produce the curves shown in Fig. 6. Analogous to Fig. 5, the dashed lines are $\langle \beta_y \rangle \pm \sqrt{\langle 2\beta_y^2 \rangle}$ and the solid lines are $\langle \beta_x \rangle \pm \sqrt{\langle 2\beta_x^2 \rangle}$. The initial phase space occupied by the electron beam is measured by the product of the initial displacement width and angular spread. In $k_\beta x, x'$ phase space, the initial gaussian phase space distribution has a circular $1/e$ contour with a radius of $5 \cdot 10^{-5}$. At the end of the undulator, the beam centroid has wandered 1.6 times its $1/e$ width in angular space and 3 times its $1/e$ width in displacement space, but its width has remained constant.

In Fig. 7 we compare $\langle x^2 \rangle^{1/2}$ to the value computed by FELEX. Because the noise in this quantity that arises from a single random undulator is too great for direct comparison, we average over sets of undulators. Here, we have taken two sets of 10 undulators each and have plotted their average standard deviation as broken lines in Fig. 7. The solid line is that expected by the ensemble averaged result obtained earlier.

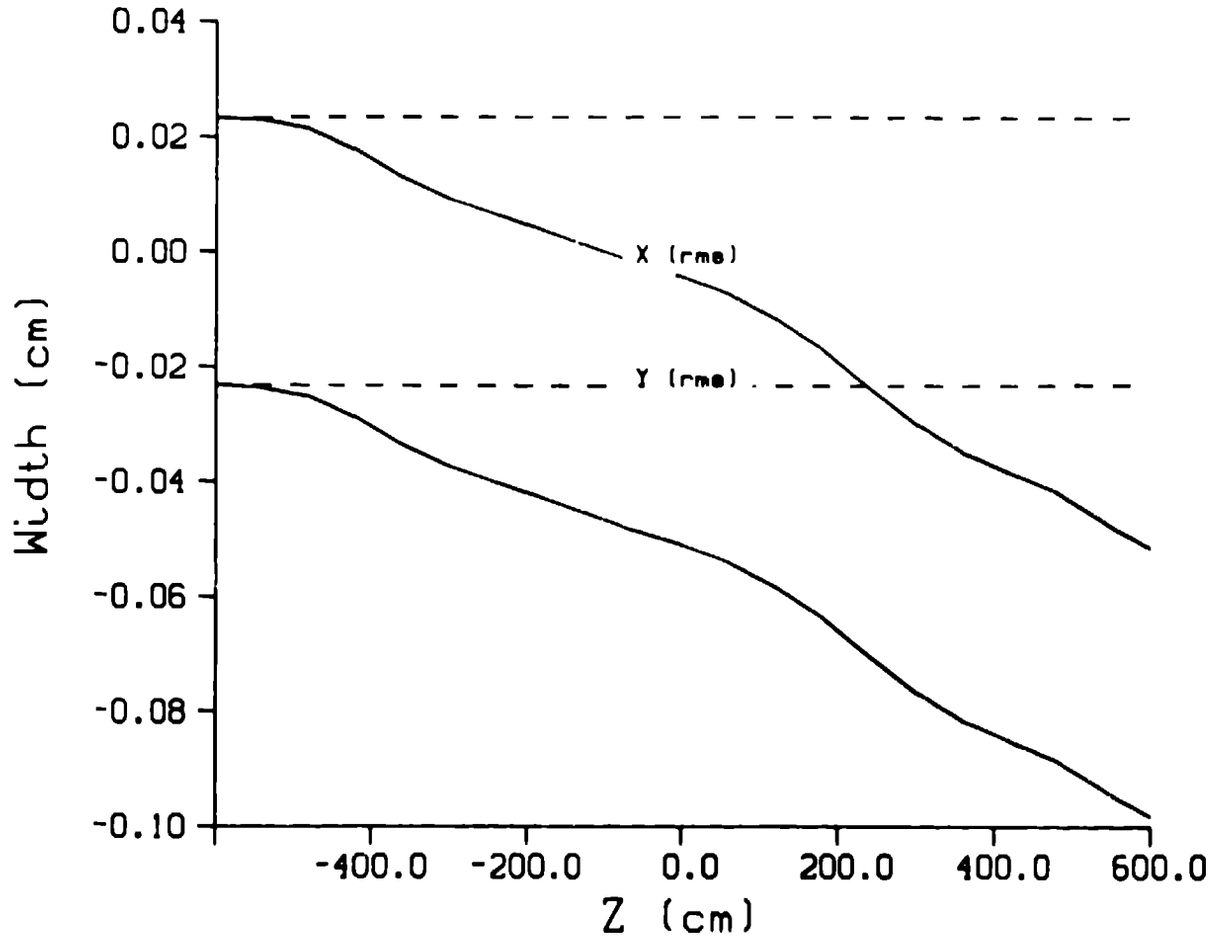

Fig. 5. Plot of the wander of the x and y edges (see text) of the electon beam versus the longitudinal location.

A collection of twenty random undulators with σ 0.1% were used to generate the gain plot shown in Fig. 8. The calculations were at the wavelength that maximized the gain in the absence of undulator field errors. Here, the gain that occurs is plotted against $\langle x \rangle_{max}$, the maximum displacement of the centroid over the length of the undulator. Considerable variation occurs from the value of 4.8, the gain without errors, to below 1.0 where absorption occurs. Also plotted is the optical waist at the center of the undulator and at the ends of the undulator. The plot shows that many of the undulators produced e-beam centroid wander that was well outside the peak of the optical mode. Hence the radiation into the opitcal mode was reduced, leading to the lower gain as $\langle x \rangle_{max}$ increased. On several of these cases, the effect of the shift of the wavelength for optimal gain was examined. The gain, maximized over wavelength, moved all of the gain values higher. A number of those with gains in the 2 to 4 range moved roughly 2/3 of the way toward the gain of 4.8.

The effect of a solenoidal magnetic field is shown in Fig. 9. The undulator chosen for this study has the worst $\langle x \rangle_{max}$ value of the set of 20 previously studied. It was this case that was shown in Figs. 5 and 6. In Fig. 9, it is seen that the gain (maximized

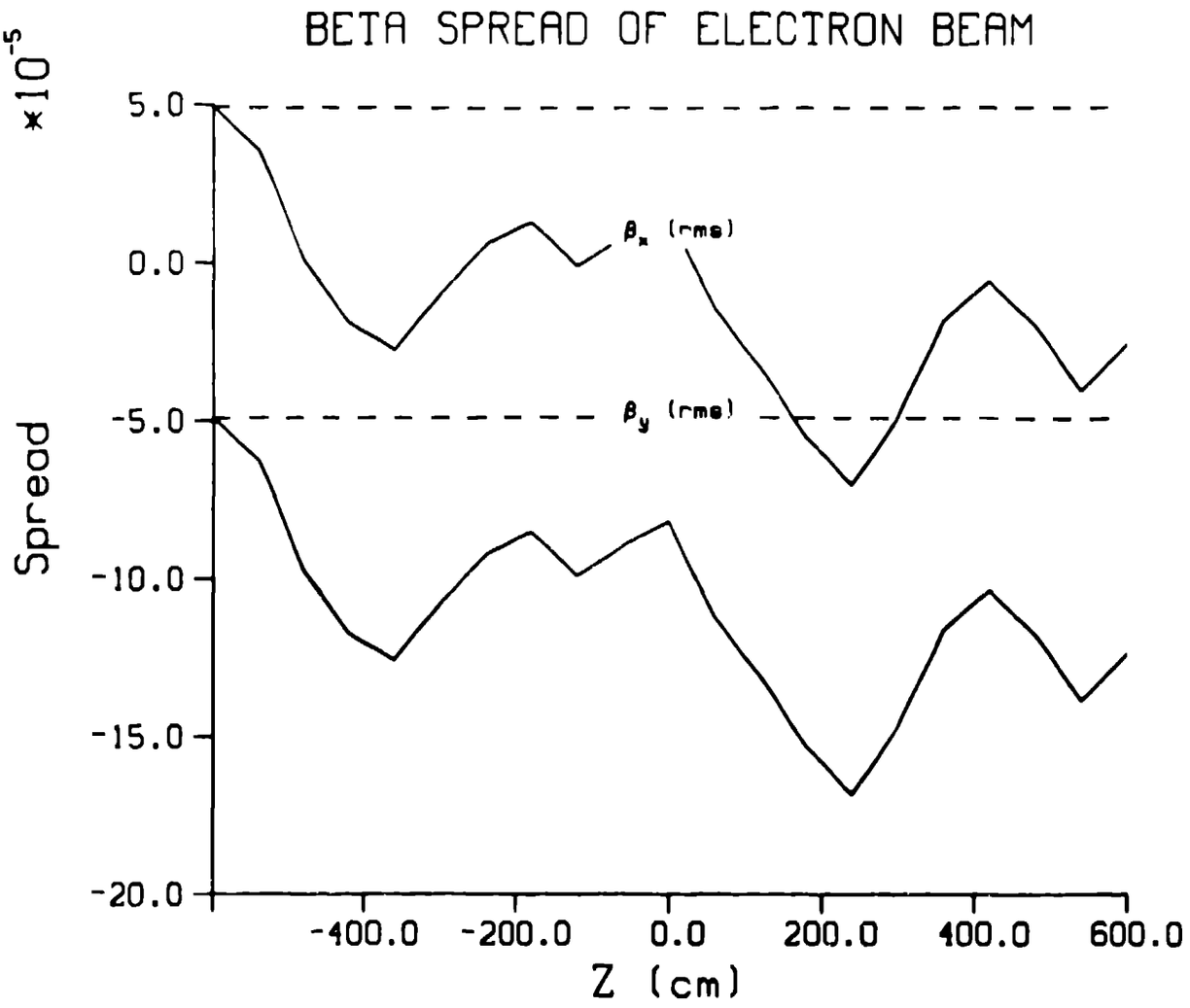

Fig. 6. Plot of the wander in angle space of the edges of the electron beam

over wavelength) increases up to an axial field value of ≈ 1 Tesla. Examination of x plotted versus z shows that at B_z 1.1T, $\langle y' \rangle_{max} \approx \langle x' \rangle_{max}$ 2.0 · 10 $^{-2}$ compared to $\langle y \rangle_{max}$ 0., $\langle x \rangle_{max}$ 7.5 · 10 $^{-2}$ at B_z 0. At the value of B_z 2T, although $\langle y' \rangle_{max} \approx \langle x' \rangle_{max}$ has decreased to 9.8 · 10 $^{-3}$, $\langle \beta_y \rangle_{max} \approx \langle \beta_x \rangle_{max}$ 16.8 · 10 $^{-5}$, and the increase in the angular centroid is more detrimental to the gain than the improvement from the displacement centroid. This result for a particular random undulator contrasts with the results averaged over an ensemble of undulators reported in the section on a solenoid with balanced focusing. On the basis of that work, we would have expected the ensemble averaged gain to increase monotonically with B_z. It would saturate at the point where displacement errors become small compared to angular errors, i.e. where Ω was several $k_\beta c$. The down turn we see in Fig. 9, must then be attributed to an interplay of the solenoidal field and the particular manifestation of field errors for this case. For other cases, then, we would expect the details of the down turn and the subsequent upturn to

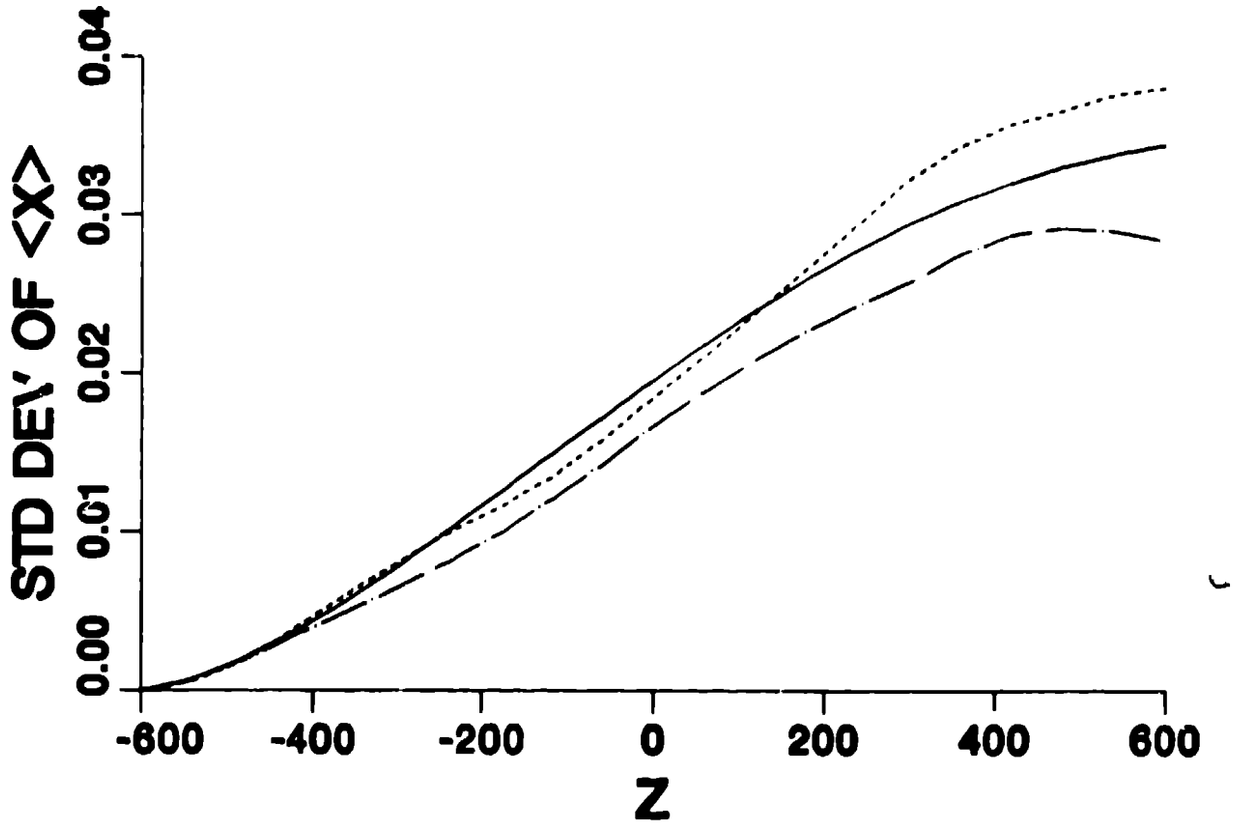

Fig. 7. A comparison between the theoretical solid curve of the standard deviation of the centroid and two averages over sets of 10 cases

be different.

Because solenoidal fields cannot completely correct the gain in these cases, we consider the addition of corrector segments. This type of improvement has been employed in the THUNDER undulator[1] at STI. The concept is shown in Fig. 10. The undulator is divided into a number of equal segments. At the end of each segment is a means of measuring the e-beam position. We also assume there is some way of measuring the angle that the e-beam is making with the x axis, although this measurement is not required in the simplest correction scheme. At the beginning of each segment is a correction coil that can steer the electron beam by giving it a programmable transverse kick. A means of making these measurements simultaneously is given in the paper in this conference by Warren and Elliott[10].

Two ways of using the measurements to determine the required transverse correction impulse are shown in Fig. 11. This plot shows the $k_\beta x, x'$ phase space. If no field errors were present, the electron beam centroid would be at the origin. The field errors that are present have moved the electron beam centroid to some random location we have labeled as E. Ideally we would like to be able to move E to the origin, but this is not possible because the transverse kick given at the beginning of the segment does not access all of

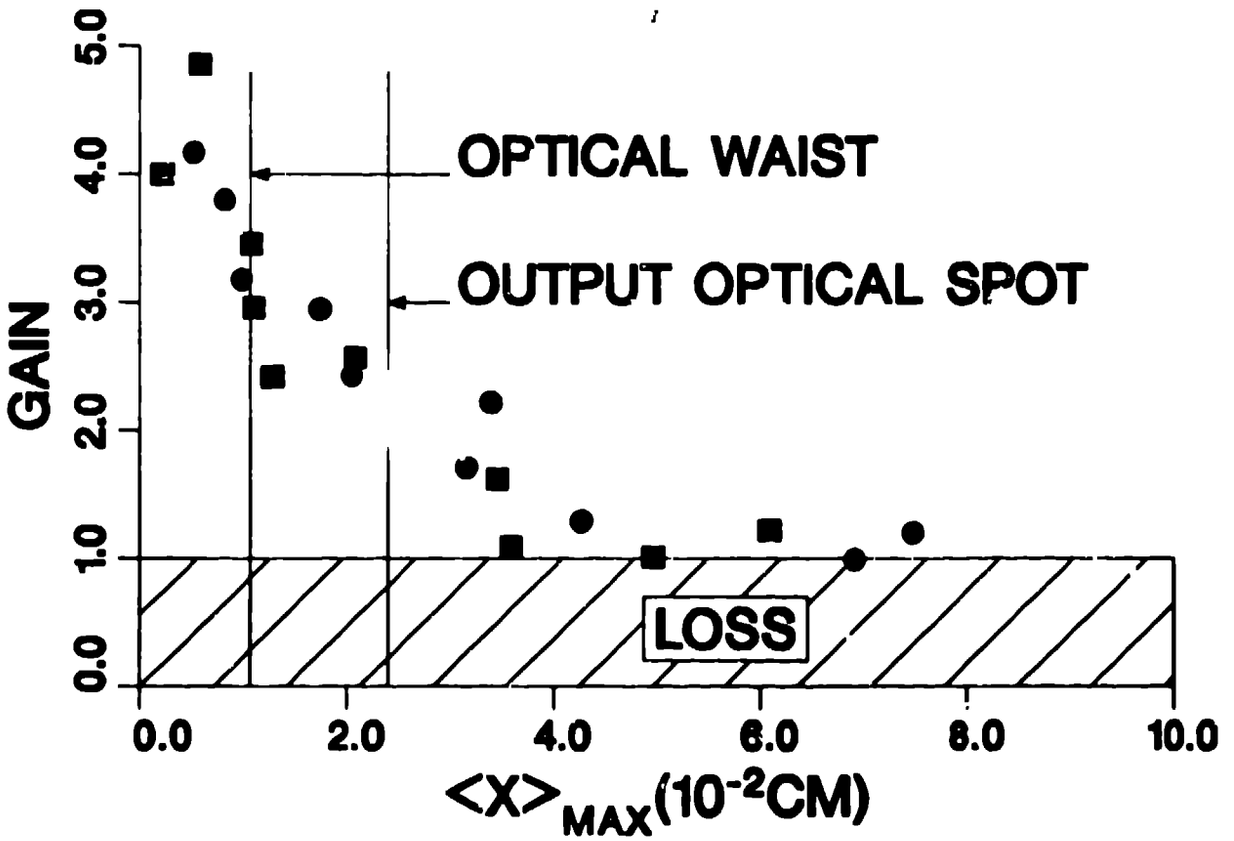

Fig. 8. A plot of the gain of different random undulators versus the maximum transverse wander of the centroid

phase space. If we assume there are no field errors present in the system, we can easily determine what part of phase space is accessed from the origin by the correction kick. The kick is initiated at the beginning of the segment, where it is manifest as a pure angular change along the x' axis. This angular change follows the betatron motion as it moves through the wiggler. This motion is the arc of a circle that is shown in Fig. 11 as moving to point C, having gone a particular fraction of a betatron period corresponding to the length of the segment. This fraction is the same irrespective of the size of the initial correction kick, and thus, the space accessed by the initial kick is a line drawn through the origin that goes through point C. This line is called the corrector line. Now we reconsider the presence of magnetic field errors. The effect of the errors and the correction kick add linearly. That means that if the system is at point E, all points accessible from point E by means of the initial correction kick lie along the line parallel to the correction line. The dashed line in Fig. 11 shows the portion of phase space accessible from E. The next question we wish answer is: To where on the dashed line do we want to correct the system. We show two choices. The first choice is shown by the point E'. It is the point along the dashed line that is nearest to the origin. Along the access line, it chooses the point that makes $|x'^2 + k_{\beta x}^2 x^2|$ a minimum. The second correction scheme is shown in Fig. 11 as point E''. This point is

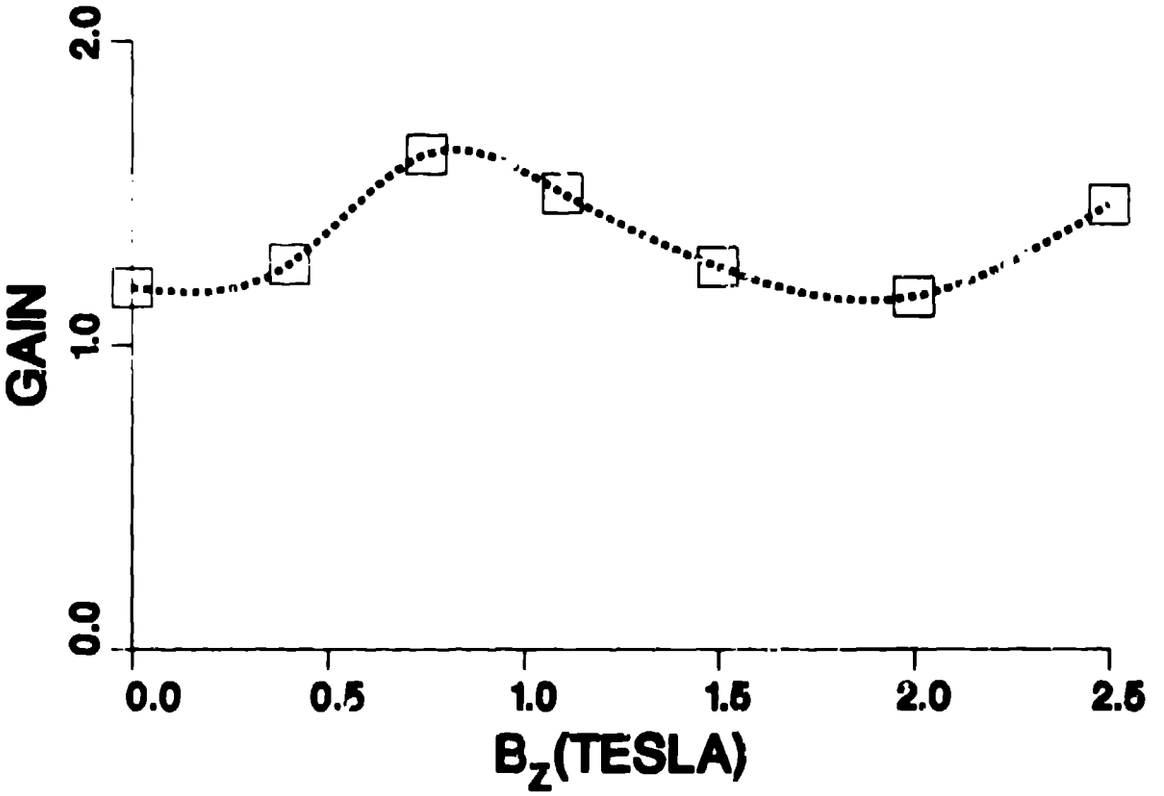

Fig. 9. A plot of the gain of one random undulator versus the axial field strength

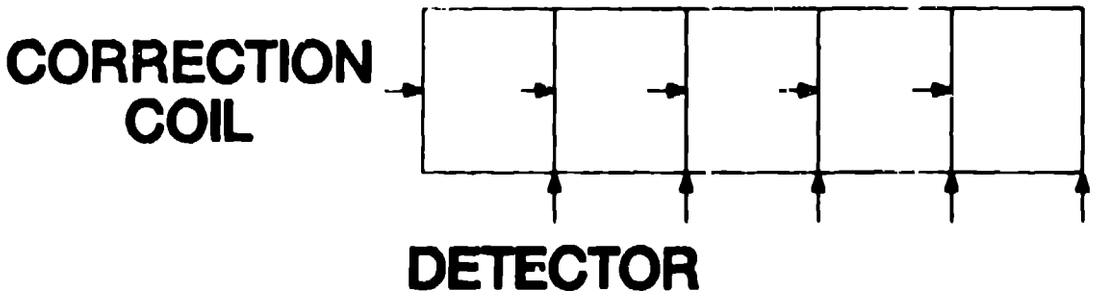

Fig. 10. Schematic of the steering error corrector scheme. Correction coils are located at the beginning of each of the 5 segments and position and angular detectors are located at the end of each segment.

chosen as the intersection of the dashed line with the y axis, i.e. it drives the x coordinate to 0. Although the distance from the origin is greater in this second method, we will show it to be a superior means of correcting the undulator. The second method is also simpler because it requires only the measurement of the x coordinate and not the angle.

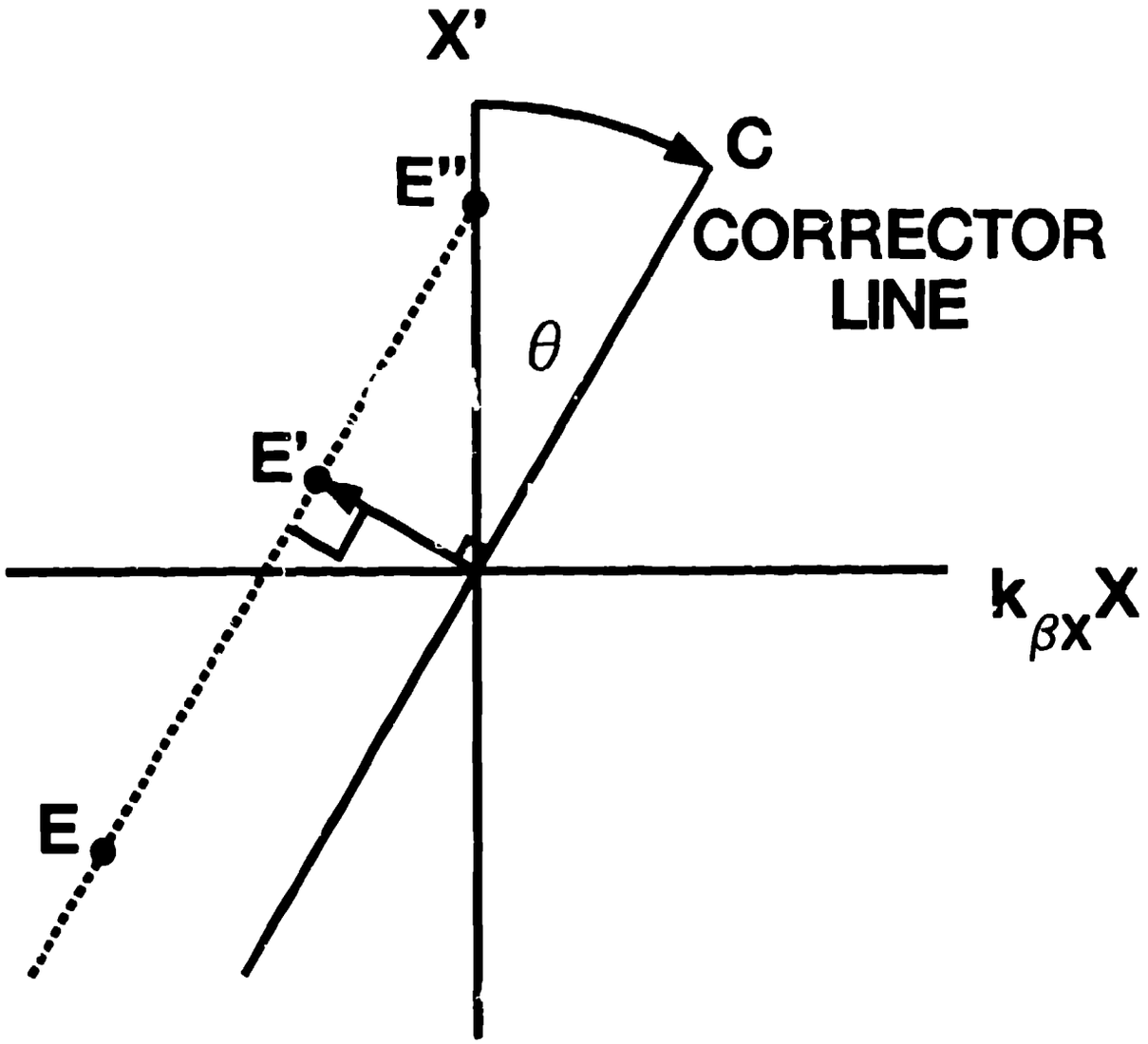

Fig. 11. An illustration of two corrector schemes in phase space. The dashed line is the part of phase space accessable from the error point E. The point E' minimizes the distance to the origin, and the point E'' makes the x coordinate 0.

The superiority of the $x \to 0$ scheme is shown in Fig. 12. This illustration shows the effect of application of corrector segments to the worst case of Fig. 7 corresponding to the undulator used in Figs. 5 and 6. The gain is computed at the frequency that maximizes the gain when no field errors are present. This gain is plotted against the number of correcting segments. For the $x \to 0$ scheme, 5 correcting segments are required to bring the gain within 10% of that occurring without field errors. On the other hand, greater than twice that number are required for the minimum distance in phase space method. It is concluded that both of these schemes permit complete correction of the undulator, and the $x \to 0$ is the better scheme.

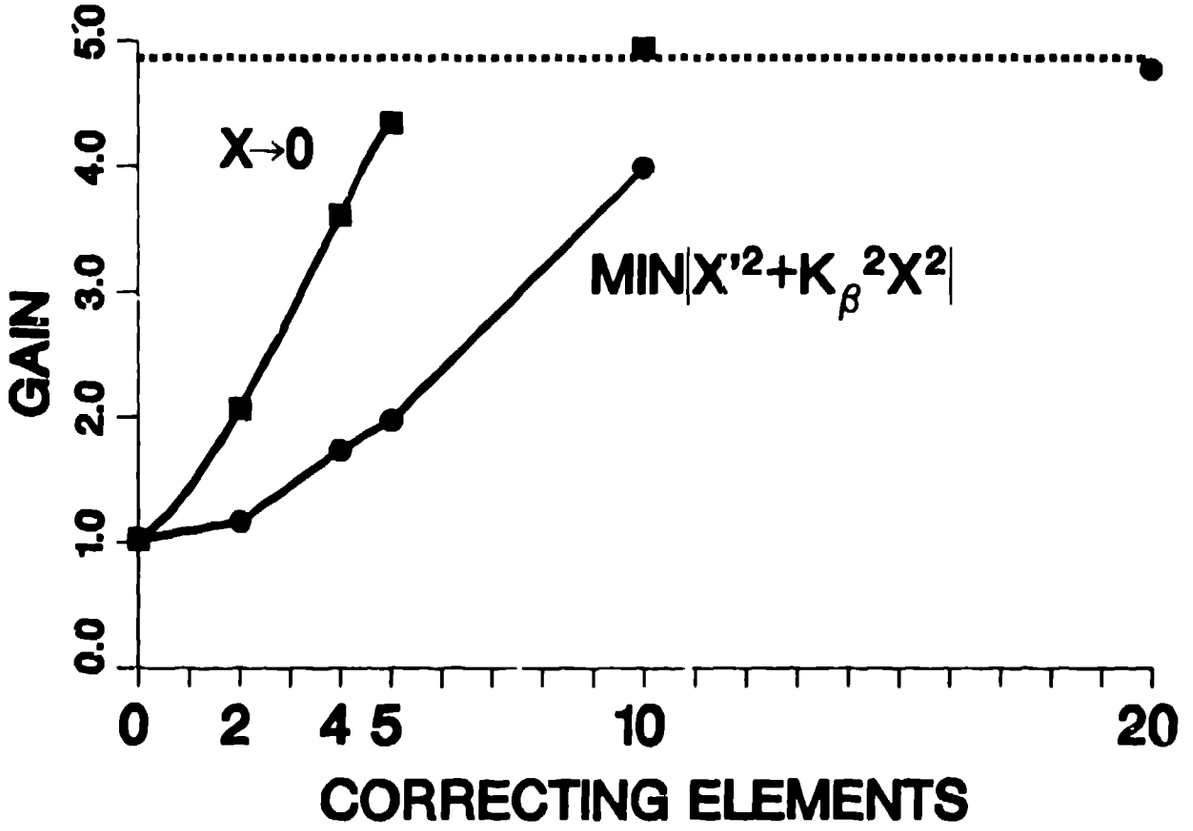

Fig. 12. The gain of a random undulator as a function of the number of correcting segments

Now we consider the combination of an easily obtainable error level of 0.7% with $x \to 0$ corrector segments. In this study, we allow the random undulator to choose the wavelength that optimizes the gain. We consider undulators with 32 corrector segments whose data points are represented by solid circles in Fig. 13. We also consider undulators with 8 segments, and those data points are shown as solid squares. For 10 different random undulators in each class, we compute the peak gain. We also compute a quantity, ϕ_l, analogous to Φ/c for a single electron. Here ϕ_{lc} is computed using the centroid quantities $\langle x \rangle$ and $\langle \beta_x \rangle$,

$$\phi_{lc} \quad \frac{k_x}{2} \int_0^{L_w} (\langle \beta_x \rangle^2 + k_{\beta x}^2 \langle x \rangle^2) dz.$$

The ensemble average of ϕ_{lc} is Φ_{lc} for the centroid motion. We have enough segments that we are on the lower portion of the curve shown in Fig. 3. There is a strong correlation between the gain and ϕ_{lc} shown in Fig. 13. The ensemble average of this quantity varies inversely with the number of segments and one segment has a value that is 1/3 that without corrector segments. The expected value for 32 segments is shown for comparison at the base of the graph. Here we see that with 32 corrector segements, Φ_{lc} 2rad, and all ten of the random undulators are within 10% of the error-free gain. Clearly, 8 corrector segments

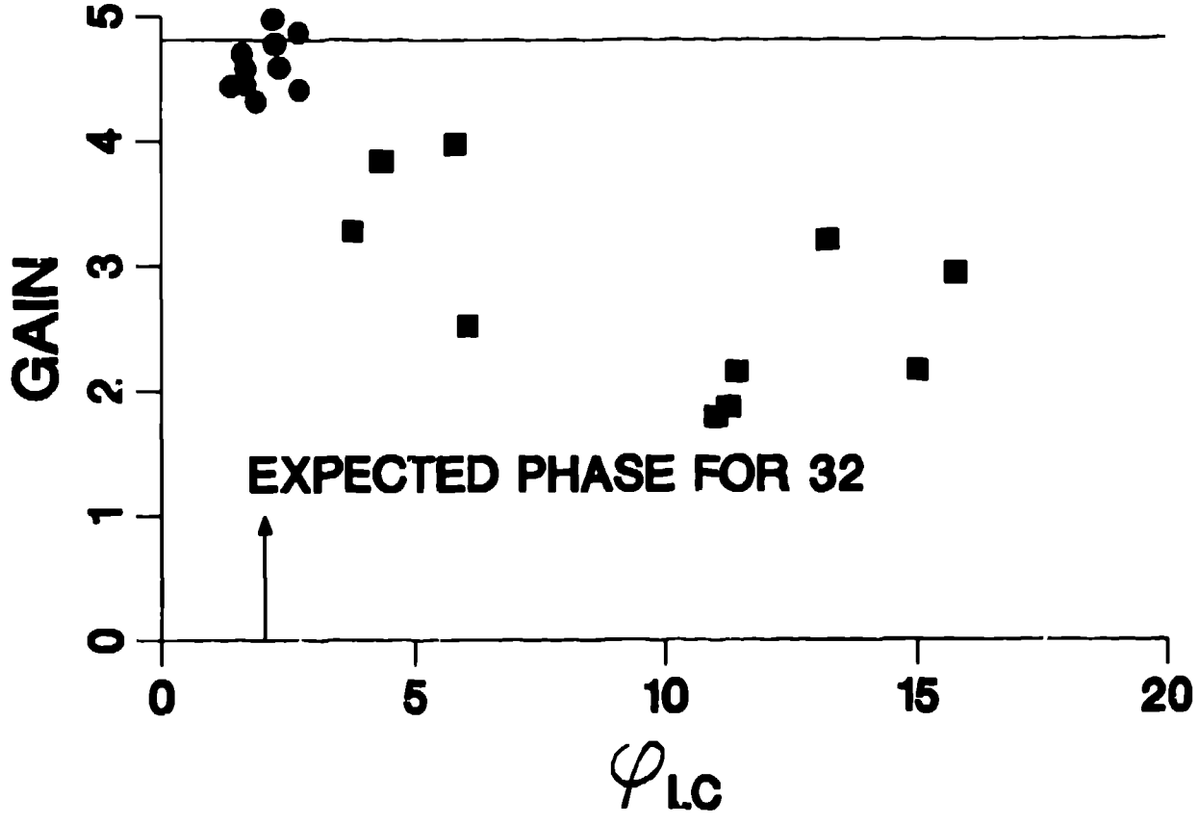

Fig. 13. Gain plotted against the longitudinal coherence phase for two configurations of correcting segments. The solid circles are for 32 correcting segments, and the solid squares are for 8 correcting segments. The arrow indicates the expected value of the longitudinal phase for 32 segments.

are insufficient to correct the undulator at this random error level.

Finally, we would like to point out that there are a number of effects we have not considered in these calculations. First, the errors considered are taken to be random and extend for half a undulator period. In an undulator, the angular errors are proportional to $\int B_y dl$. Thus, if there are two half-period segments that have errors in the opposite direction, the resultant error will be less than random. In building an undulator, one is cognizant of this property and deliberately cancels errors of these types. Consequently, the field error level is not an adequate measure of the quality of an undulator. The correlation of successive errors must be considered, and the effective random error can be considerably less than that measured for the field. Our advanced state of the art case is therefore within reason. Secondly, no measurement is completely precise. In the correction scheme where we take $x \to 0$, there is always a residual error. We have tacitedly assumed that we have a measurement precision that makes little change from perfect precision. This will be true if the measurement precision is good enough to make $(k_s L_w/2)(2k_{\beta x}^2/3 + 2/L_c)2\sigma_x^2$ small compared to Φ_{LC} and σ_x small compared to w_0, the optical spot size, where σ_x is the

displacement error and L_c is the length of the correction station.

Conclusions

We have studied the influence of parameters of magnetic field errors for XUV FELs. The measure of the longitudinal coherence phase, Φ_l, is one important parameter. In the [illegible] case, we see that the spontaneous emission intensity for a cold beam drops to 90% of its peak for $\Phi_l \approx 6.7$rad. We showed that for long undulators, beam wander is the important criterion, but for segmented undulators with short segments longitudinal coherence is the important criterion. We showed that a small improvement can occur when wander dominates by the application of a solenoidal guiding magnetic field. By far, the more effective way to control field errors is by the segmentation of the undulator. Without segmentation and with field errors of $\sigma \approx 0.1\%$, the achievement of 90% of the error free gain is unlikely in the 120mm device. Either an improvement in σ or segmentation can reduce these requirements. With field errors at $\sigma \approx 0.7\%$, we have shown segmentation can reduce the field errors to acceptable levels. For this case, $\Phi_l \approx 2$rad. These conclusions are subject to the qualifications and the model specified in the body of this paper, and these will be the subject of future investigations.

References

1. K. E. Robinson, D. C. Quimby, and J. M. Slater, The Tapered Hybrid Undulator (THUNDER) of the Visible Free-Electron Laser Oscillator Experiment. To appear in **JQE**.1987. K. E. Robinson and D. C. Quimby, Canted-Pole Transverse Gradients in Planar Undulators. Particle Accelerator Conference, Washington DC, 16-19 march 1987, to be published in **IEEE Trans. Nucl. Sci.** K. E. Robinson, D. C. Quimby, J. M. Slater, T. L. Churchill, and A. S. Valla, Field Certification of a High Strength Tapered Hybrid Undulator. Eight International Free Electron Laser Conference, Glasgow, Scotland, 1-5 September, 1986, to appear in **Nuclear Instruments and Methods in Physics Research.** J. M. Slater, Undulator Development at Spectra Technology, Undulator magnets for Synchrotron Radiation and Free Electron Lasers, 23-26 June, Trieste, Italy, to appear in **Physics Scripta.**
2. B. M. Kincaid, Random Errors in Undulators and their Effects on the Radiation Spectrum, **J. Opt. Soc. Am. B/2** 1294-1306, 1985. B. M. Kincaid, The TOK Undulator, Undulator magnets for Synchrotron Radiation and Free Electron Lasers, 23-26 June, Trieste, Italy, to appear in **Physics Scripta.**
3. J. M. J. Madey, Conceptual System Design of XUV FEL's, in **Free Electron Generation of Extreme Ultraviolet Coherent Radiation**, J. M. J. Madey and C. Pellegrini, eds. (American Institute of Physics, New York,1984), pp.12-43.
4. K. Halbach, Permenant Magnet Undulators, **Jour. de Phys.** Colloque C1, 44 211-216, 1983. K. Halbach, Physical and Optical Properties of Rare Earth Cobalt Magnets, **Nuclear Instru. and Methods** 187 109-117, 1981.
5. J. C. Goldstein, B. D. McVey, and B. E. Newnam, Three-Dimensional Simulations of an XUV Free-Electron Laser, **SPIE** 582 350-360, 1985.
6. J. D. Jackson,**Classical Electrodynamics, Second Edition**, (John Wiley and Sons, New York, 1975), p.671.
7. J. C. Goldstein, B. E. Newnam, R. K. Cooper, and J. C. Comly, Jr., An XUV/VUV Free-Electron Laser Oscillator, **Second Topical Meeting on Laser Techniques in the Extreme Ultraviolet**, Boulder, CO, March 5-7, 1984, appearing as AIP Conference Proceedings No. 119, Subseries on Optical Science and Engineering No. 5, **Laser Techniques in the Extreme Ultraviolet** eds. S. E. Harris and T. B. Lucatorto (American Institute of Physics, New York, 1984) pp.293-303.
8. E. T. Scharlemann, Wiggle Plane Focusing in Linear Wigglers, **J. Appl. Phys.** 58 2154-2161, 1985.
9. Gary Deis, FEL Wiggler Development at LLNL, Undulator magnets for Synchrotron Radiation and Free Electron Lasers, 23-26 June, Trieste, Italy, to appear in **Physics Scripta**.
10. R. Warren and C. J. Elliott, A New System for Wiggler Fabrication and Testing, Undulator magnets for Synchrotron Radiation and Free Electron Lasers, 23-26 June, Trieste, Italy, to appear in **Physics Scripta**.